Perfectly matched layer in numerical wave propagation: factors that affect its performance

Arti Agrawal and Anurag Sharma

The perfectly matched layer (PML) boundary condition is generally employed to prevent spurious reflections from numerical boundaries in wave propagation methods. However, PML requires additional computational resources. We have examined the performance of the PML by changing the distribution of sampling points and the PML's absorption profile with a view to optimizing the PML's efficiency. We used the collocation method in our study. We found that equally spaced field sampling points give better absorption of beams under both optimal and nonoptimal conditions for low PML widths. At high PML widths, unequally spaced basis points may be equally efficient. The efficiency of various PML absorption profiles, including new ones, has been studied, and we conclude that for better numerical efficiency it is important to choose an appropriate profile.

OCIS codes: 000.4430, 350.5500.

1. Introduction

In recent years, methods for propagating beams numerically have gained importance for design and analysis of optical waveguides and devices. These methods directly give the total picture of a field as it propagates through a waveguide, which may have a complicated structure involving several branches and variations in physical characteristics. Some of these methods are the fast-Fourier-transform beam-propagation method,[1] the finite-difference beam-propagation method,[2] and the collocation method.[3–7]

One of the major problems with any beam propagation method is that the infinite transverse extent of space has to be represented by a finite domain bounded by numerical boundaries. In these methods the numerical boundary is represented by the extreme points on which the field is sampled. Because the whole numerical scheme is generally lossless, the total energy within the numerical window remains the same, and hence any wave that in reality should leave the numerical window region is directed back into the numerical window, thereby representing an unreal phenomenon. The conventional way to reduce the effect of this problem is to put a strongly absorbing medium of appropriate thickness at the edge of the window, thereby imposing the so-called absorbing boundary condition.[8–11] Another way is to use the so-called transparent boundary condition[12–14] in which the parameters of the wave near the edge of the window are so modified for a given angle of incidence that it represents an outgoing plane wave at that angle. Both of these methods have been successful to a limited extent. Some time ago, Berenger[15] introduced the concept of a perfectly matched layer (PML) for application with finite-difference time domain (FDTD) solutions of Maxwell's equations. In the PML method a layer of a specially designed anisotropic medium is put at the edge of the window. The absorption profile in this window can be arbitrarily chosen, subject to certain conditions. The PML boundary condition was found to be highly effective for applications to optical wave propagation.[11,16–20] Huang *et al.*[16] first applied the PML in the beam propagation method and also showed its use in modal analysis of optical waveguides in which the PML was found to be effective in the computation of leaky modes.[17] Zhou *et al.*[18] developed the PML boundary condition for the scalar FDTD. Chew and Weedon[19] showed that modifying Maxwell's equations and adding extra degrees of freedom permit the specification of absorbing boundaries with zero reflection for all angles of incidence and frequencies. Chen *et al.*[20] introduced the modified PML, which permits effective absorption of the evanescent mode energy.

The authors are with the Department of Physics, Indian Institute of Technology, Delhi, New Delhi-110 016, India. A. Sharma's e-mail address is asharma@physics.iitd.ac.in.

Received 3 October 2003; revised manuscript received 19 March 2004; accepted 28 April 2004.

0003-6935/04/214225-07$15.00/0

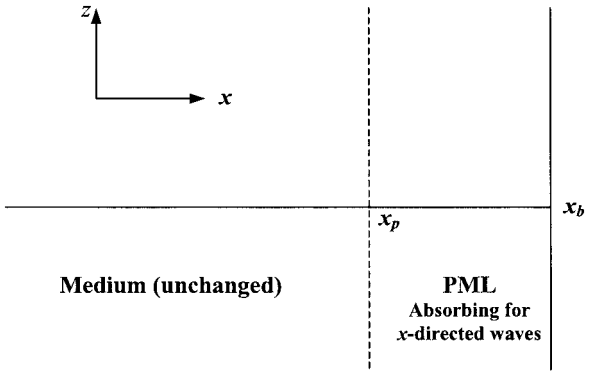

Fig. 1. Geometry of implementation of the PML technique.

In any implementation of the PML method (or any other method), one seeks to increase the absorption of the undesired reflections as well as to keep the layer as thin as possible so as not to increase the computation effort significantly. In this respect, the design of the absorption profile of the PML assumes significance. Further, in the numerical beam propagation methods the points on which the field is sampled are generally taken equally spaced. However, in a number of cases unequally spaced points have also been tried, with a distinct computational advantage.

We have implemented the PML boundary condition in the collocation methods of beam propagation and have found it effective. Using this implementation, we investigated the effect of distribution of sample points on the PML's performance. Finally, we investigated the influence of various absorption profiles in the PML, including a new type of absorption profile.

2. Perfectly Matched Layer Technique

In the PML technique, a layer of an artificial anisotropically absorbing medium that strongly absorbs the waves propagating along the x direction but does not absorb the waves propagating along the z direction (which is the general direction of propagation) is introduced at the edge of the numerical window.[11,15] Further, the layer is matched perfectly at the interface with the real window, so there are no reflections from there. The perfectly matched layer is implemented as a variable transformation in which the transverse coordinate x becomes complex, with the imaginary part increasing gradually as one moves into the layer.[11] Thus we introduce a transformation (see Fig. 1)

$$x = h(\sigma), \tag{1}$$

with

$$\begin{aligned} h(\sigma) &= \sigma && \sigma < x_p \\ &= x_p + \int \xi[1 - ip(\xi)]\mathrm{d}\xi && x_p < \sigma < x_b, \end{aligned} \tag{2}$$

where $\xi = \sigma - x_p$, x_p is the edge of the real medium, and x_b is the edge of the numerical window. The absorption profile function $p(\xi)$ should be such that $p(0) = 0 = p'(0)$ for perfect matching at $x = x_p$. The region up to x_p is termed the real window, whereas the region between x_p and x_b is the PML.

A variety of profiles have been described in the literature.[18,19] These are all power-law profiles, including square, cubic, and quartic profiles:

$$p(\xi) = p_0\xi^q, \qquad q = 2, 3, 4, \ldots . \tag{3}$$

It has been shown that for FDTD schemes the quartic profile is better than the usual square profile.[18,21] However, for continuous wave propagation problems, generally the square profile has been used. We investigated various power-law profiles for the wave propagation problems. We also investigated a new profile:

$$p(\xi) = p_0 \sin^q(\pi\xi/2\delta), \qquad q = 2, 3, 4, \ldots , \tag{4}$$

where δ is the width of the PML layer and q defines the shape of the profile. By appropriate choice of power q, strength p_0, and width $\delta = x_p - x_b$ of the PML, the wave can be absorbed to a desired level to reduce reflections into the computation window.

4. Collocation Method

For simplicity, we confine our discussion to two-dimensional waveguides; however, the method discussed can be extended to three-dimensional structures. A two-dimensional waveguide structure is defined by its refractive-index distribution $n^2(x, z)$. The electromagnetic fields that propagate through such a dielectric structure must satisfy Maxwell's equations. However, in a majority of practical waveguiding structures (we confine our discussion to such cases) the relative variation of the refractive index is sufficiently small to allow the scalar wave approximation to be made. It then suffices to consider instead a much simpler Helmholtz equation:

$$\frac{\partial^2\Psi}{\partial x^2} + \frac{\partial^2\Psi}{\partial z^2} + k_0{}^2 n^2(x, z)\Psi(x, z) = 0, \tag{5}$$

where $\Psi(x, z)$ represents one of the Cartesian components of the electric field (generally referred to as the scalar field). The time dependence of the field has been assumed to be $\exp(i\omega t)$, and $k_0 = \omega/c$ is the free-space wave number.

In the collocation method, we express the unknown field as a linear combination over a set of orthogonal basis functions $\phi_n(x)$:

$$\Psi(x, z) = \sum_{n=1}^{N} c_n(z)\phi_n(x), \tag{6}$$

where $c_n(z)$ are the expansion coefficients, n is the order of the basis functions, and N is the number of basis functions used in the expansion. The choice of $\phi_n(x)$ depends on the boundary conditions and the symmetry of the guiding structure. The coefficients of expansion $c_n(z)$ are unknown and represent the variation of the field with z. In the collocation method, one can effectively obtain these coefficients

by requiring that the differential equation, Eq. (5), be satisfied exactly by the expansion, Eq. (6), at N collocation points $x_j, j = 1, 2, \ldots, N$, which are chosen such that these are the zeros of $\phi_{N+1}(x)$. Thus, using this condition and with some algebraic manipulations,[3–6] one converts the wave equation, Eq. (5), into an ordinary differential matrix equation:

$$\frac{d^2\mathbf{\Psi}}{dz^2} + [\mathbf{S}_0 + \mathbf{R}(z)]\mathbf{\Psi}(z) = 0, \tag{7}$$

where

$$\mathbf{\Psi}(z) = \begin{bmatrix} \Psi(x_1, z) \\ \Psi(x_2, z) \\ \vdots \\ \Psi(x_N, z) \end{bmatrix},$$

$$\mathbf{R}(z) = k_0^2 \begin{bmatrix} n^2(x_1, z) & 0 & \cdot & 0 \\ 0 & n^2(x_2, z) & \cdot & \cdot \\ \cdot & \cdot & \cdot & 0 \\ 0 & \cdot & 0 & n^2(x_N, z) \end{bmatrix}, \tag{8}$$

and $\mathbf{S}_0$ is a known constant matrix defined by the basis functions. We refer to Eq. (7) as the collocation equation. In deriving this equation from the wave equation, Eq. (5), we made no approximation except that N is finite and that Eq. (7) is exactly equivalent to Eq. (5) as $N \to \infty$. Thus the accuracy of the collocation method improves indefinitely as N increases.

In the collocation method, one can either solve the collocation equation directly or invoke the paraxial approximation, if it is valid, to obtain the equation for the envelope:

$$\frac{d\chi}{dz} = \frac{1}{2ik}[\mathbf{S}_0 + \mathbf{R}(z) - k^2\mathbf{I}]\chi(z), \tag{9}$$

where $\chi(z) \equiv \mathbf{\Psi}(z)\exp(ikz) = \mathrm{col}[\chi(x_1, z)\ \chi(x_2, z) \cdots \chi(x_N, z)]$ and $\mathbf{I}$ is a unit matrix. This equation can be solved directly by use of, e.g., the Runge–Kutta method or of the operator method as in the fast-Fourier-transform beam-propagation method. The latter procedure has been shown to be unconditionally stable numerically.[6]

A unique feature of the collocation method is that one obtains an equation as a result that can be solved or modified in a variety of ways. It can be solved as an initial-value problem by use of any standard method such as the Runge–Kutta method[3–5] or the predictor–corrector method. In the paraxial form it can also be solved by matrix operator methods based on the approach of symmetrized splitting of the sum of two noncommutating operators.[6] One could also use to advantage a suitable transformation of the independent or the dependent variable or both. Indeed, it has been shown[7] that a transformation could be used to redistribute the collocation points (which are the field sampling points in the transverse cross section) in such a way that the density of points increases in and about the guiding region, and the transverse extent, covered by the sampled field, also increases.

A. Equally Spaced Sample Points

The electric field can be expressed in terms of plane waves that can further be expressed in terms of sinusoidal functions. These sinusoidal functions are solutions of the Helmholtz equation for a homogeneous medium. These functions oscillate even at $x \to \infty$ in order that the field vanish at large distances; we assume an artificial boundary at $\pm L$ where the field is assumed to vanish. With these boundary conditions the Helmholtz equation for a homogeneous medium gives solutions that vary as

$$\begin{aligned} \phi_n(x) &= \cos(v_n x), \qquad n = 1, 3, 5, \cdots N - 1, \\ \phi_n(x) &= \sin(v_n x) \qquad n = 2, 4, 6, \cdots N, \end{aligned} \tag{10}$$

where $v_n = n\pi/2L$. The collocation points are then the equally spaced zeros of $\cos(v_{N+1}x)$ for an even N; thus, $x_j = [(2j/N + 1) - 1]L, j = 1, 2, 3 \cdots, N$. In this case, matrix $\mathbf{S}_0$ is given by

$$\mathbf{S}_0 = \mathbf{AHA}^{-1}, \tag{11}$$

where $\mathbf{A} = \{A_{ij}{:}A_{ij} = \phi_j(x_i)\}$ and $\mathbf{H} = \mathrm{diag}(-v_1^2 - v_2^2 - v_3^2 \cdots - v_N^2)$. Thus the collocation equation, Eq. (9), is fully defined and can be solved numerically for a given $n^2(x, z)$.

B. Unequally Spaced Sample Points

For unequally spaced sample points we choose the expansion functions to be Hermite–Gauss functions such that

$$\phi_n(x) = \mathsf{N}_{n-1}H_{n-1}(\alpha x)\exp(-\tfrac{1}{2}\alpha^2 x^2), \tag{12}$$

where N_{n-1} is the normalization constant and α is an adjustable parameter. The collocation points are now given by

$$H_N(\alpha x_j) = 0, \qquad j = 1, 2, \ldots, N. \tag{13}$$

The Hermite polynomial H_N defined above has N distinct zeros, which are unequally spaced. Matrix $\mathbf{S}_0$ in this case is given by

$$\mathbf{S}_0 = \mathbf{D}_1 - \mathbf{AD}_2\mathbf{A}^{-1}, \tag{14}$$

where

$$\begin{aligned} \mathbf{D}_1 &= \alpha^4 \times \mathrm{diag}(-x_1^2 - x_2^2 \cdots - x_N^2), \\ \mathbf{D}_2 &= \alpha^2 \times \mathrm{diag}(1\ldots3\ldots5\ldots2N - 1), \\ \mathbf{A} &= \{A_{ij}{:}A_{ij} = \phi_j(x_i)\}. \end{aligned} \tag{15}$$

4. Implementation of the Perfectly Matched Layer by Use of the Variable Transformation

It was shown earlier[7] that one can easily implement a variable transformation in the collocation method. Therefore we have implemented the PML technique by using the variable transformation given in Section 2, using the formalism outlined below.

We implemented the PML by transforming Eq. (5), using

$$x = h(\sigma),$$
$$\psi(x, z) = \sqrt{h'(\sigma)}U(\sigma, z), \tag{16}$$

where $h(\sigma)$ is defined in Eq. (2). Equation (5) then became

$$\frac{\partial^2 U}{\partial z^2} + f(\sigma)\frac{\partial^2 U}{\partial \sigma^2} + [g(\sigma) + k_0{}^2 n^2(\sigma, z)]U(\sigma, z) = 0, \tag{17}$$

where

$$f(\sigma) = [h'(\sigma)]^{-2}, \tag{18}$$

$$g(\sigma) = \frac{1}{2h'^4}\left(h'''h' - \frac{3}{2}h''^2\right), \tag{19}$$

where a prime denotes differentiation with respect to σ. Equation (17) is similar to Eq. (5) in form, except for a factor $f(\sigma)$ in the second term. We can therefore use the collocation method of Sec. 3 to convert Eq. (17) into a matrix equation[7]:

$$\frac{d^2\mathbf{U}}{dz^2} + [\hat{\mathbf{S}}_0 + \mathbf{R}(z)]\mathbf{U}(z) = 0. \tag{20}$$

The vector $\mathbf{U}(z) = \{U_j : U_j = U(\sigma_j)\}$ denotes the values of the transformed field at the collocation points, and matrix $\hat{\mathbf{S}}_0$ is given by

$$\hat{\mathbf{S}}_0 = \mathbf{F}\mathbf{D}_1 - \mathbf{F}\mathbf{A}\mathbf{D}_2\mathbf{A}^{-1} + \mathbf{G}, \tag{21}$$

where $\mathbf{F} = \{F_j : F_j = f(\sigma_j)\}$, $\mathbf{G} = \{G_j : G_j = g(\sigma_j)\}$, and $\mathbf{A}$, $\mathbf{D}_1$, and $\mathbf{D}_2$ are defined in Eq. (15) above, except that now x is replaced by σ. Using the paraxial approximation for the envelope, $\hat{\chi}(z) \equiv \mathbf{U}(z)\exp(ikz)$, we obtain the equation

$$\frac{d\hat{\chi}}{dz} = \frac{1}{2ik}[\hat{\mathbf{S}}_0 + \mathbf{R}(z) - k^2\mathbf{I}]\hat{\chi}(z). \tag{22}$$

Equation (22) can be solved as an initial-value problem by use of any standard method such as the Runge–Kutta method or the predictor–corrector method. We have used the fourth-order Runge–Kutta method in our examples. It may be noted that, in the real window, the fields $U(\sigma)$ and $\psi(x)$ are identical; hence, $\hat{\chi}$ directly gives χ, which is the quantity of interest.

5. Numerical Examples and Results

The effectiveness of the PML layer depends on the distribution of the sampling points and on thickness of the PML as well as on its absorption profile $p(\xi)$. To assess the performance of a PML we studied the absorption of a Gaussian beam launched at different angles with the z axis in a medium of index 1.4472. The width of the beam is 4 μm, and the wavelength of light is 1.31 μm. As a measure of absorption in the PML, we computed the energy remaining in the real window. With reference to Fig. 2, the beam is launched at point A at an angle θ with the z axis. The beam would hit the edge of the numerical window at point B and get reflected to reach point C, situated exactly above point A in Fig. 2. Thus, if point A is at a distance x_A from the edge of the numerical window, the total distance propagated along z would be $AC = 2x_A \cot\theta$. The fractional power remaining in the real window at $z = AC$ has been used as a measure of the absorption by the PML; this is designated E_R. Ideally, for total absorption, $E_R = 0$. In most figures E_R has been plotted for different parameters. In some figures, however, the fractional power remaining in the real window has been plotted as a function of the propagated distance z; this is designated E_z. For each PML width and the tilt angle of the beam, we obtained the value of p_0 by minimizing the value of E_R. Such a layer is termed an optimized PML layer for that angle.

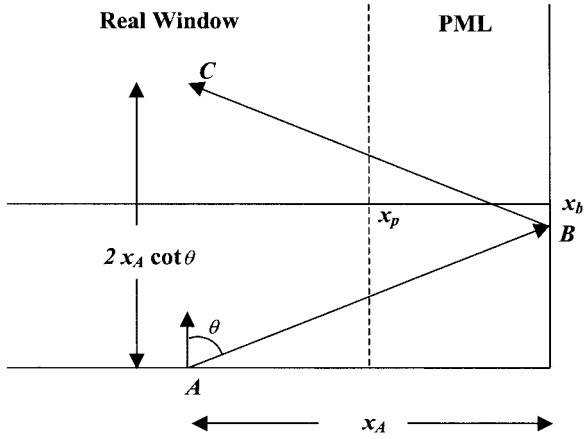

Fig. 2. Geometry of the definition of E_R.

We have computed E_R in order to compare the various absorption profiles. By using both Hermite–Gauss and sinusoidal bases we explored the effect of point distribution on the PML profiles. In all calculations, the total width of the numerical window is $\sim$44.6 μm and the number of sample points is $N = 100$.

A. Distribution of Sampling Points

In Fig. 3 we have plotted E_R as a function of PML width (expressed in percentage of the total window size) for the beam tilted at 25° with respect to the z axis, for equal and unequal sampling points. The PML has a square absorption profile, and each individual PML layer was optimized to absorb the incident beam. It can be seen quite clearly that, with increasing PML width, E_R decreases for both equally and unequally spaced points. However, in equally spaced points, E_R is much lower, by $\sim$3 orders of magnitude at the lowest PML width, than in the unequally spaced points. For other widths also, the absorption is better for equally spaced sample points, though for larger PML widths equally spaced points and unequally spaced points perform nearly equally well.

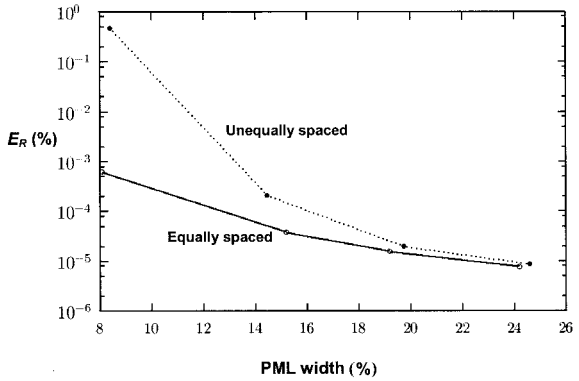

Fig. 3. Energy remaining in the real window, E_R (in %), as a function of the PML width (% of the total numerical window) for the square profile with the unequally spaced and equally spaced distributions of sample points.

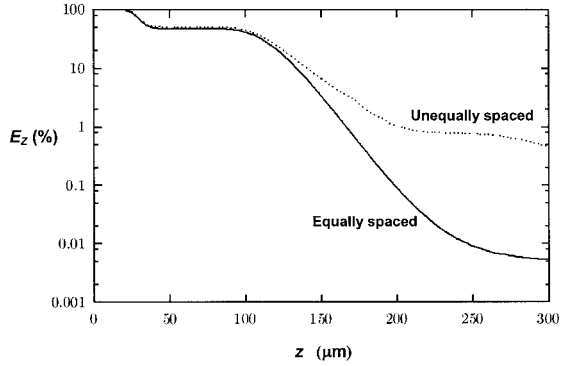

Fig. 5. Energy remaining in the real window, E_z (in %), as a function of propagation distance z. Results are shown for square profiles with unequally spaced and equally spaced distributions of sample points. The PML width is 3.5 μm (8% of the total window).

To test performance under nonoptimum conditions we optimized the layer for absorption at a given angle of the beam and then propagated beams at other angles. Figure 4 shows the results for the square absorption profile. The layer is optimized for a tilt angle of 25°. It can be seen that, for unequally spaced points, as the angle deviates from 25°, E_R increases rapidly. But in equally spaced points, even as the angle increases, E_R varies much less. Thus with equally spaced points the PML can better absorb beams at angles other than the one for which the layer is optimized.

The final test is absorption of two beams incident onto the PML at different angles simultaneously. The layer is optimized to absorb a beam at 22.5°, and we consider the propagation of two beams, tilted at 15° and 30°, whose widths are 4 and 2 μm, respectively. Figures 5 and 6 show the variation of E_z for equally spaced as well as unequally spaced points, for layers of widths 3.5 μm (8% of the total window) and 6.7 μm (15% of the total window), respectively. The beam tilted at the higher angle hits the PML first and gets absorbed first, so we see a decrease in E_z, which then becomes somewhat constant, whereas the second beam continues to travel in the real window for some more distance. When the second beam also hits the PML, E_z again starts decreasing. The important point to note is that at lower PML width (Fig. 5) E_z is lower by almost 3 orders of magnitude in the equally spaced basis, whereas performance is comparable in both cases at higher width (Fig. 6). The two figures also show that the PML's absorptivity is much more sensitive to width when the points are unequally spaced, whereas with equally spaced points the PML's performance is not affected as much with change in width. Thus, at lower PML width, the use of equally spaced points has a distinct advantage in reducing reflected energy under optimum as well as nonoptimum conditions. For larger widths, the PML's performance for the two types of point distribution is comparable.

One can understand the difference in PML performance for the two types of point distribution with reference to Fig. 7, in which we have plotted absorption profiles for the two point distributions that correspond to Fig. 3 for 8% PML width. The figure shows that for the unequally spaced points the profile is steeper and the number of points is 6, whereas in the case of the equally spaced points the profile is less

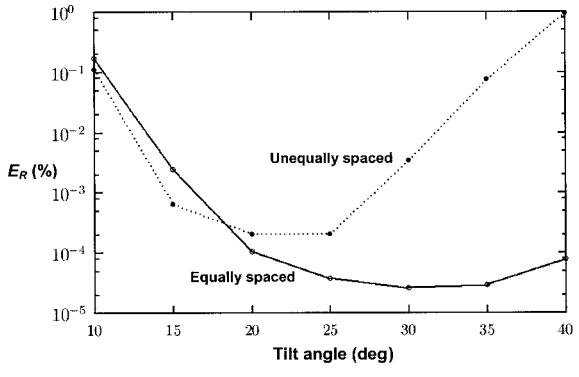

Fig. 4. Energy remaining in the real window, E_R (in %), as a function of beam tilt angle for the square profile with unequally spaced and equally spaced distributions of sample points.

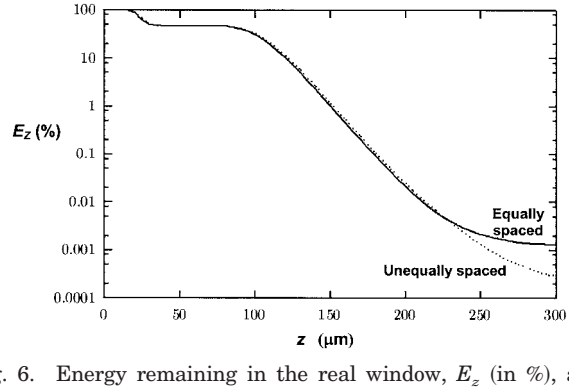

Fig. 6. Energy remaining in the real window, E_z (in %), as a function of propagation distance z. Results are shown for square profiles with unequally spaced and equally spaced distributions of sample points. The PML width is 6.7 μm (15% of the total window).

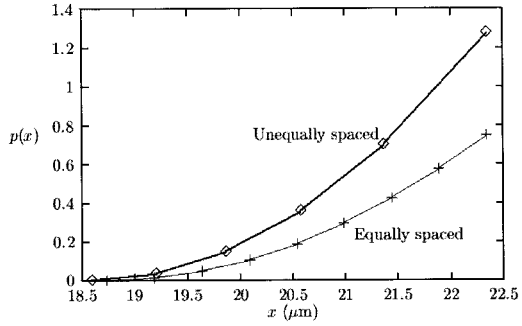

Fig. 7. Square absorption profile in the unequally and the equally spaced point distributions for PML width 8%.

steep and the number of points is 9 (although the total number of sample points in the entire computation domain is the same, in an unequally spaced point distribution the number of points in the guiding region is increased, leaving fewer points near the edge of the window). This means that for unequally spaced points the change in the value of $p(x)$ from one sample point to the next is large compared with that for the equally spaced point distribution. Thus there is a stronger discretization for unequally spaced points. It was shown by Vassallo and Collino[11] that such a discretization leads to reflections. A stronger discretization gives larger reflections. This argument is further strengthened by Fig. 8, in which we have plotted the absorption profile for the two point distributions that correspond to Fig. 3 for 19% PML width. The figure shows that the number of points is nearly equal in the two cases and that the steepness is also similar, making the discretization error similar in the two cases. The result is that the value of E_R is nearly same for both types of point distribution (see Fig. 3).

B. Absorption Profile

We next examine the effect of the absorption profile on the performance of the PML. We consider the power-law profiles [Eq. (3)], which have been used commonly, and also consider the new sine power-law profile [Eq. (4)] in our investigation. Figure 9 shows

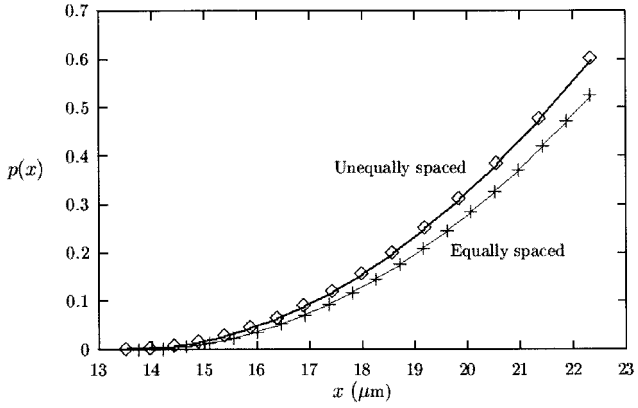

Fig. 8. Square absorption profile in the unequally and the equally spaced point distributions for PML width 19%.

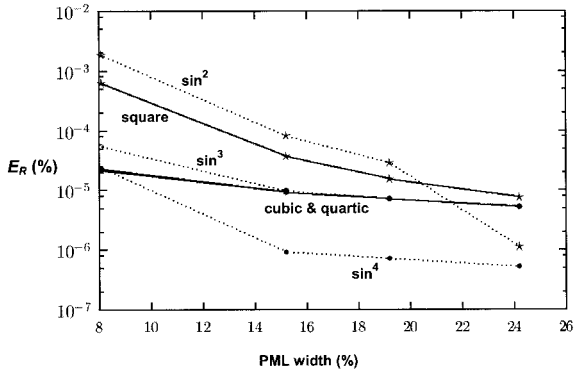

Fig. 9. Energy remaining in the real window, E_R (in %), as a function of PML width (%) for several absorption profiles with equally spaced point distributions.

a plot of E_R as a function of the PML width for several profiles for equally spaced points, and Fig. 10 shows the same results for unequally spaced points. In the case of equally spaced points, the $\sin^4$ profile is by far the best, at all widths. The cubic, quartic, and the $\sin^3$ profiles perform similarly, and square and $\sin^2$ are by far the worst. With unequally spaced points, however, quartic and $\sin^4$ profiles are worst at lower width, and square and $\sin^2$ are best. At higher widths, all the profiles show E_R values saturated to nearly the same value when there are unequally spaced points. Comparing these two figures, we can conclude that, for all profiles, at lower width, an equally spaced basis is better, and with this point distribution a steeper profile $\sin^4$ is the best among all the profiles investigated.

The above results show that for smaller widths of the PML it is important to choose a correct point distribution, which is equally spaced at least for the example that we have chosen, and an appropriate absorption profile, which is $\sin^4$ for our example. Of course, one could choose a large (20–25%) PML width and not worry about the specifics of the point distribution and the absorption profile; however, the penalty would be a larger computation window and a larger computational effort. For repetitive computations, as in the case of a typical design exercise, it

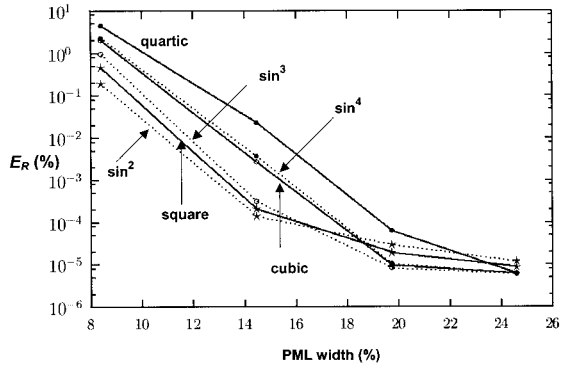

Fig. 10. Energy remaining in the real window, E_R (in %), as a function of PML width (%) for several absorption profiles with unequally spaced point distributions.

would pay to follow the first option of using a lower PML width with appropriately chosen point distribution and absorption profile.

6. Summary and Conclusions

The perfectly matched layer boundary condition has been implemented in the collocation method for equally spaced and unequally spaced distributions of sample points. We studied the performance of the PML as an absorbing layer for a Gaussian beam as a test case. The effects of different distributions of sample points and of different PML absorption profiles on PML performance have thus been studied. We found that equal spacing between points leads to better absorption of beams under both optimal and nonoptimal conditions for lower PML widths. At higher PML widths, unequally spaced and equally spaced points perform equally well. The PML performance is a strong function of the absorption profile for smaller (and hence, numerically more efficient) PML widths, whereas for larger widths the nature of the absorption profile matters much less. For smaller widths, a newly suggested $\sin^4$ absorption profile with equally spaced points gives the best PML performance. For better numerical efficiency, one would like to use smaller PML widths; for optimized performance of the PML, it would be important to choose an appropriate point distribution and absorption profile.

This research was partially supported by grant 03(0976)/02/EMR-II from the Council of Scientific and Industrial Research (CSIR), India. A. Agrawal is a CSIR research fellow.

References

1. M. D. Feit and J. A. Fleck, Jr., "Light propagation in graded-index optical fibers," Appl. Opt. **17,** 3990–3998 (1978).
2. C. L. Xu and W. P. Huang, "Finite-difference beam propagation methods for guided-wave optics," in *Methods for Modeling and Simulation of Optical Guided-Wave Devices*, W. Huang, ed., Vol. 11 of Progress in Electromagnetic Research (EMW, Cambridge, Mass., 1995), pp. 1–49.
3. A. Sharma, "Collocation method for wave propagation through optical waveguiding structures," in *Methods for Modeling and Simulation of Optical Guided-Wave Devices*, W. Huang, ed., Vol. 11 of Progress in Electromagnetic Research (EMW, Cambridge, Mass., 1995), pp. 143–198.
4. S. Banerjee and A. Sharma, "Propagation characteristics of optical waveguiding structures by direct solution of the Helmholtz equation for total fields," J. Opt. Soc. Am. A **6,** 1884–1894 (1989).
5. A. Sharma and S. Banerjee, "Method for propagation of total fields or beams through optical waveguides," Opt. Lett. **14,** 94–96 (1989).
6. A. Sharma and A. Taneja, "Unconditionally stable procedure to propagate beams through optical waveguides using the collocation method," Opt. Lett. **16,** 1162–1164 (1991).
7. A. Sharma and A. Taneja, "Variable-transformed collocation method for field propagation through waveguiding structures," Opt. Lett. **17,** 804–806 (1992).
8. E. L. Lindman, "Free space boundary conditions of the time dependent wave equation," J. Comput. Phys. **18,** 66–78 (1975).
9. B. Engquist and A. Majda, "Absorbing boundary conditions for the numerical simulation of waves," Math. Comput. **31,** 629–651 (1977).
10. G. Mur, "Absorbing boundary condition for the finite-difference approximation of the time-domain electromagnetic-field equations," IEEE Trans. Electromagn. Compat. **EMC-23,** 377–382 (1981).
11. C. Vasallo and F. Collino, "Highly efficient absorbing boundary conditions for the beam propagation method," J. Lightwave Technol. **14,** 1570–1577 (1996).
12. G. R. Hadley, "Transparent boundary condition for beam propagation," Opt. Lett. **16,** 624–626 (1991).
13. G. R. Hadley, "Transparent boundary condition for the beam propagation method," Opt. Lett. **28,** 624–626 (1992).
14. G. R. Hadley, "Transparent boundary condition for the beam propagation method," IEEE J. Quantum Electron. **28,** 363–370 (1992).
15. J. P. Berenger, "A perfectly matched layer for the absorption of electromagnetic waves," J. Comput. Phys. **114,** 185–200 (1994).
16. W. P. Huang, C. L. Xu, W. Lui, and K. Yokoyama, "The perfectly matched layer (PML) boundary condition for the beam propagation method," IEEE Photon. Technol. Lett. **8,** 649–651 (1996).
17. W. P. Huang, C. L. Xu, W. Lui, and K. Yokoyama, "The perfectly matched layer boundary condition for modal analysis of optical waveguides: leaky mode calculations," IEEE Photon Technol. Lett. **8,** 652–654 (1996).
18. D. Zhou, W. P. Huang, C. L. Xu, D. G. Fang, and B. Chen, "The perfectly matched layer boundary condition for scalar finite-difference time-domain method," IEEE Photon. Technol. Lett. **13,** 454–456 (2001).
19. W. C. Chew and W. H. Weedon, "A 3D perfectly matched medium from modified Maxwell's equations with stretched coordinates," Microwave Opt. Technol. Lett. **7,** 599–604 (1994).
20. B. Chen, D. G. Fang, and B. H. Zhou, "Modified Berenger PML absorbing boundary condition for FD–TD meshes," IEEE Microwave Guided Wave Lett. **5,** 399–401 (1995).
21. J. C. Chen and K. Li, "Quartic perfectly matched layers for dielectric waveguides and gratings," Microwave Opt. Technol. Lett. **10,** 319–323 (1995).